▌ Imaging Agents

BODIPY Dyes Bearing Multibranched Fluorinated Chains: Synthesis, Structural, and Spectroscopic Studies**

Maria I. Martinez Espinoza,[a] Lorenzo Sori,[a] Andrea Pizzi,[a] Giancarlo Terraneo,[a] Ivana Moggio,[b] Eduardo Arias,[b] Gianluca Pozzi,[c] Simonetta Orlandi,[c] Valentina Dichiarante,[a] Pierangelo Metrangolo,[a] Marco Cavazzini,*[c] and Francesca Baldelli Bombelli*[a]

Abstract: A small series of boron-dipyrromethene (BODIPY) dyes, characterized by the presence of multibranched fluorinated residues, were designed and synthesized. The dyes differ in both the position (*para*-perfluoroalkoxy-substituted phenyl ring or boron functionalization) and number of magnetically equivalent fluorine atoms (27 or 54 fluorine atoms per molecule). Photophysical and crystallographic characterization of the synthesized BODIPYs was carried out to evaluate the effect of the presence of highly fluorinated moieties on the optical and morphological properties of such compounds.

Introduction

Boron-dipyrromethene (BODIPY) dyes are a well-known class of fluorophores, in which the complexation of a substituted dipyrrin with boron trifluoride results in a planar rigid cyanine structure.[1] This imparts outstanding photophysical properties to BODIPYs, namely, narrow Gaussian-shaped absorption and emission bands, which are associated with high absorption coefficients and generally high emission quantum yields.[1b, 2] Furthermore, they show moderate redox potentials and excellent thermal and photochemical stabilities.[1a–c] Over the last few years, the versatility and robustness of BODIPYs have also been widely exploited in optoelectronic and photonic applications, spanning from the preparation of photovoltaic cells[3] to their use as organic semiconductors in organic field-effect transistors (OFETs)[4] and as organic solid-state dye laser materials.[5] Considering their remarkable stability over a wide range of pH

and inertness to changes in the physiological environment, it is not surprising that BODIPYs also significantly contribute to the development of bioimaging systems and diagnostic tools.[6]

The most attractive aspect of BODIPYs for bioimaging relies on the possibility of tailoring their optical and physical properties simply by introducing different substituents at specific positions of the dye core.[7] For example, higher quantum yields can be obtained by increasing the rigidity of the BODIPY core,[7b–d] whereas nonradiative deactivation pathways result from distortion of the BODIPY backbone.[1b] Their absorption and emission spectral features can be easily pushed to the far-red region by extending electronic delocalization of the structures.[7b,e–i] Overall, chemical functionalization of the core and conjugation with specific functional groups allow for the fine-tuning of the spectroscopic characteristics for application as either sensors for chemical and biological targets or small fluorescent tags for molecules, macromolecules, nanocarriers, and so forth.[6b, 8]

Multimodal BODIPY-based imaging agents have also been developed[6a, 9] covering various imaging techniques, such as magnetic resonance imaging (MRI) and ultrasound (US) imaging.[10] Among noninvasive imaging techniques, ^{19}F-MRI is emerging as a powerful quantitative detection modality for clinical use because it permits in-depth in vivo detection with high spatial resolution, without the use of radioactive agents.[11] In particular, the combination of ^{19}F-MRI with fluorescence imaging (FLI) allows simultaneously in vivo tracking (^{19}F-MRI/FLI) and ex vivo intracellular localization (FLI); thus providing in-depth in vivo detection, higher sensitivity, and real-time responses.[11b,c] Accordingly, the integration of typical characteristics of an efficient ^{19}F-MRI contrast agent, that is, an appropriate number of magnetically equivalent fluorine atoms in the BODIPY core, would result in an efficient dual modality (^{19}F-

[a] Dr. M. I. Martinez Espinoza, Dr. L. Sori, Dr. A. Pizzi, Prof. Dr. G. Terraneo, Dr. V. Dichiarante, Prof. Dr. P. Metrangolo, Prof. Dr. F. Baldelli Bombelli
Laboratory of Supramolecular and Bio-Nanomaterials (SupraBioNanoLab), Department of Chemistry, Materials, and Chemical Engineering "Giulio Natta", Politecnico di Milano
20131 Milan (Italy)
E-mail: francesca.baldelli@polimi.it

[b] I. Moggio, E. Arias
Departamento de Materiales Avanzados
Centro de Investigación en Química Aplicada, 25294 Saltillo (México)

[c] Dr. G. Pozzi, Dr. S. Orlandi, Dr. M. Cavazzini
Institute of Molecular Science and Technologies (ISTM)
National Research Council (CNR), 20133 Milan (Italy)
E-mail: marco.cavazzini@istm.cnr.it

[**] BODIPY = boron-dipyrromethene.

Supporting information and the ORCID identification number(s) for the author(s) of this article can be found under: https://doi.org/10.1002/chem.201901259.

MRI/FLI) imaging agent.[12] Despite the massive amount of work aimed at the structural variation of BODIPY cores, only a few examples of fluorinated BODIPYs have been reported in the literature, to date, and most of them are characterized by a low number of fluorine atoms.[13] This might be due to the environmental impact of perfluorinated compounds with linear chains longer than six carbon atoms,[14] although alternatives have been recently provided by using multibranched fluorinated compounds with ultrashort fluorinated alkyl groups.[15]

On the basis of this general framework, herein we present the synthesis and characterization of a small series of multibranched fluoroalkoxy-substituted BODIPYs (Figure 1). This mo-
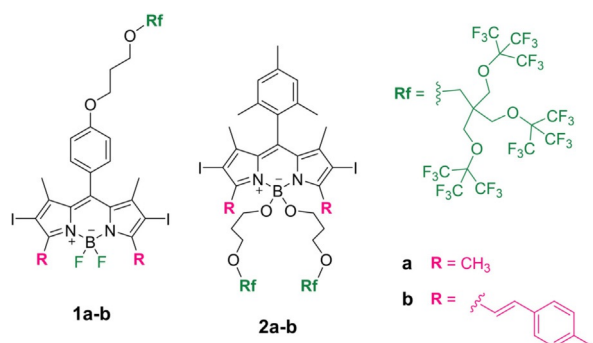

Figure 1. Chemical structures of the fluorinated BODIPY dyes synthesized and studied in this work.

lecular design multiplies the number of magnetically equivalent fluorine atoms in the molecule (27 or 54 F atoms per molecule) and guarantees a sustainable fluorous chemistry, producing degradation products with limited bioaccumulation.[16] These synthesized BODIPYs not only differ in the position and number of fluorinated residues, but also in the extension of the conjugation length of the BODIPY core (Figure 1). In particular, compounds **1a** and **1b** are characterized by a *para*-perfluoroalkoxy-substituted phenyl ring in the *meso* position of the BODIPY core, with a total of 27 magnetically equivalent fluorine atoms, whereas compounds **2a** and **2b** contain two perfluoro-*tert*-butoxy alkoxy residues bound to the boron atom, with a total of 54 magnetically equivalent fluorine atoms. Derivatives **1b** and **2b**, which have a more extended conjugation

length than that of analogues **1a** and **2a**, thanks to the introduction of styryl groups at the 3,5-positions, are also characterized by an emission spectrum in the far-red region, which is more suitable for in vivo imaging. Photophysical and crystallographic characterization of all compounds was carried out to evaluate the effect induced by the presence of highly fluorinated moieties on their optical and morphological properties.

Results and Discussion

Synthesis of fluorinated BODIPYs

In addition to the presence of one or more fluorinated residues able to provide an intense, single ^{19}F NMR signal, two other main guidelines were followed in the design of the fluorinated BODIPYs under study. First, two iodine atoms were placed on the BODIPY core to provide a dual feature: working as replaceable functional groups through orthogonal synthesis with the perspective of preparing more complex structures,[17] and promoting efficient singlet oxygen generation, similarly to previously developed halogenated BODIPYs used as effective phototherapeutic agents.[18] Second, an increased delocalization of the π electrons was pursued by extending conjugation through a condensation reaction of the acid methyl groups in the 3,5-positions of the preformed BODIPYs with a suitable aromatic aldehyde.[3, 17]

As detailed in Scheme 1, the synthesis of dyes **1a** and **1b** started with the preparation of benzaldehyde **3** through the reaction of fluorinated mesylate R_f-OMs[19] with 4-hydroxybenzaldehyde. According to similar procedures, the condensation of benzaldehyde **3** with two equivalents of 2,4-dimethyl-1*H*-pyrrole, followed by treatment with dichlorodicyanobenzoquinone and complexation with boron trifluoride diethyl etherate, allowed the isolation of fluorinated BODIPY **4**. Iodination in the presence of iodic acid and iodine in hot ethanol afforded BODIPY **1a** in excellent yield. BODIPY **1b** was finally obtained by means of Knoevenagel condensation between **1a** and two equivalents of *p*-tolualdehyde.

We surmised that boron functionalization with suitable fluorinated alcohols might provide an effective and versatile way to prepare fluorinated BODIPYs by taking advantage of a large library of already available dyes.[7c, 20] Indeed, compounds **2a**
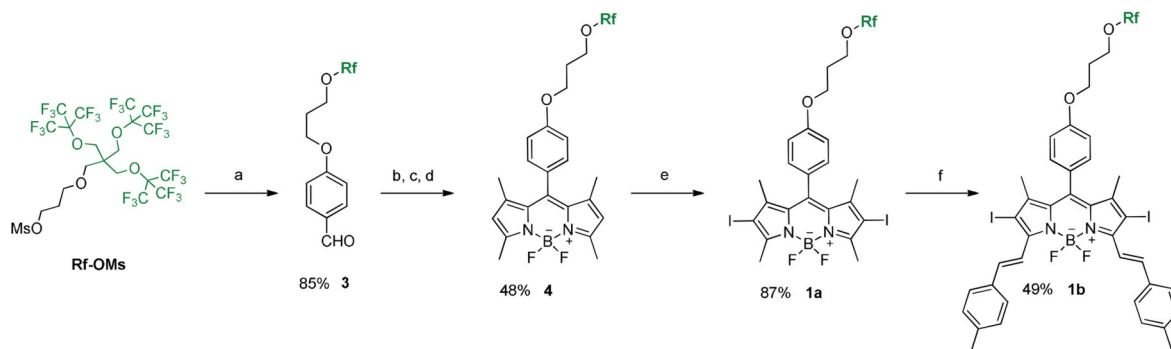
Scheme 1. Synthesis of BODIPYs **1a** and **1b**: a) 4-hydroxybenzaldehyde, K$_2$CO$_3$, DMF, 80 °C, 16 h; b) 2,4-dimethyl-1*H*-pyrrole, CF$_3$COOH, CH$_2$Cl$_2$, RT, 3 h; c) 2,3-dichloro-5,6-dicyanobenzoquinone (DDQ), 0 °C, 10 min; d) Et$_3$N, BF$_3$·O(C$_2$H$_5$)$_2$, RT, 2 h; e) HIO$_3$, I$_2$, EtOH, 60 °C, 1 h; f) *p*-tolualdehyde, pyrrolidine, AcOH, 4 Å molecular sieves, CH$_3$CN, 1 h.

and **2b** were prepared according to the route illustrated in Scheme 2. Parent BODIPY **5**[21] was iodinated in the presence of iodic acid and iodine in hot ethanol to give diiodo derivative **6** in excellent yield. Knoevenagel condensation between **6** and
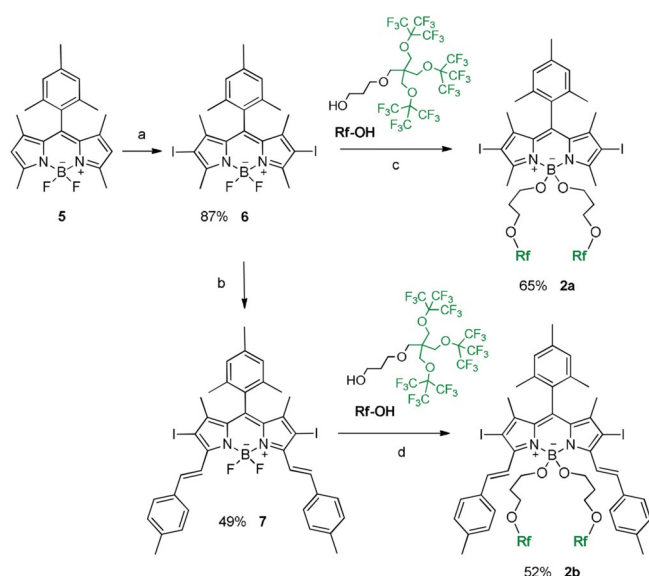
Scheme 2. Synthesis of BODIPYs **2a** and **2b**: a) HIO_3, I_2, EtOH, 60 °C, 1 h; b) *p*-tolualdehyde, pyrrolidine, AcOH, 4 Å molecular sieves, CH_3CN, 1 h; c) $AlCl_3$, CH_2Cl_2, 50 °C, 5 min; d) $AlCl_3$, THF, 60 °C, 5 min.

two equivalents of *p*-tolualdehyde, with acetonitrile as a solvent at 95 °C, in the presence of pyrrolidine and acetic acid, allowed isolation of **7**[22] in very good yield. Finally, the replacement of fluorine atoms on the parent BODIPYs **6** and **7** was achieved by treatment with $AlCl_3$ in either dry CH_2Cl_2[20b] or THF, with the subsequent addition of synthesized fluorinated alcohol R_f-OH;[19,23] thus affording **2a** and **2b** in fair yields.

Spectroscopic characterization in solution

The intrinsic photophysical properties of the fluorinated BODIPYs were determined in different solvents: THF, dichloromethane, and acetone. Only the photophysical data in THF used for further discussion herein are reported in Table 1 (see also Tables T1 and T2 in the Supporting Information for analogous results in other solvents). The optical properties of the synthe-

sized fluorinated BODIPYs are, in general, similar to those of the non-fluorinated precursors **6** and **7** (Figure S1 in the Supporting Information). In particular, for compounds **2a** and **2b**, the results are consistent with those reported in the literature; thus showing that the substitution of fluorine atoms with alkoxy groups on the boron atom does not alter the wavelength and profile of the absorption and emission spectra.[1b] All compounds exhibit a main absorption excitonic band, consistent with BODIPY optical features and attributed to the HOMO→LUMO (S_0→S_1) electronic transition,[1] with high extinction coefficients ranging from 90 000 to 140 000 M^{-1} cm^{-1}. In detail, the absorption spectra of **1a** and **2a** (Figure 2) contain narrow spectral bands with two maximal absorptions in the visible region: The intense band at $\lambda = 531$ nm corresponds to the HOMO→LUMO (S_0–S_1) transition, whereas the less pronounced shoulder at $\lambda = 500$ nm is attributed to the 0–1 vibrational transition. Additionally, a weaker broad absorption band
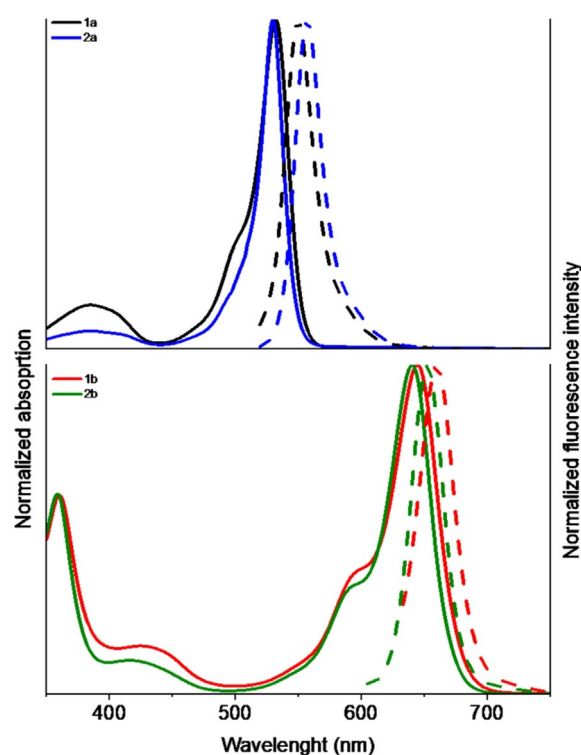

Figure 2. Absorption (solid lines) and emission (dashed lines) spectra of the four fluorinated BODIPYs in THF.

Table 1. Optical and magnetic properties of fluorinated BODIPY dyes in THF.

	λ_{max} abs [nm]	ε (10^3 M^{-1} cm^{-1})	HHBWabs[a]	λ_{max} em [nm]	Φ_F[b] [%]	$\Delta\nu$ [nm]	τ[c] [ns]	k_r	k_{nr}	T_1[d] [s]	T_2[d] [s]
6	531	76	28	551	7	20	0.80	0.09	1.16	ND[e]	ND[e]
7	645	96	40	657	27	12	1.43	0.19	0.51	ND[e]	ND[e]
1a	531	103	28	550	5	19	0.76	0.09	1.25	1.45	1.02
1b	645	99	45	657	21	12	1.44	0.15	0.55	1.37	0.60
2a	531	138	27	551	4	20	1.18	0.03	0.82	1.32	1.07
2b	640	104	42	653	27	13	1.64	0.16	0.44	1.12	0.96

[a] HHBWabs = half-height bandwidth of the absorption. [b] Relative quantum yields were determined by using rhodamine B ($\lambda_{ex} = 510$ nm) as a standard for compounds **1a** and **2a**, and methylene blue ($\lambda_{ex} = 595$ nm) as a reference for **1b** and **2b**. [c] $\lambda_{ex} = 510$ nm for **1a** and **2a**, and $\lambda_{ex} = 560$ nm for **1b** and **2b**. [d] Values of T_1 and T_2 were measured in acetone containing 10 % (v/v) [D_6]acetone for locking. [e] ND = not determined.

at shorter wavelength ($\lambda = 380$ nm) can be assigned to $S_0–S_2$ transitions.[1b] On the other hand, the absorption maxima for both **1b** and **2b** are redshifted (Figure 2), with excitonic bands at $\lambda = 645$ and 640 nm and the first vibrational replica at $\lambda = 595$ nm. Styryl-functionalized BODIPYs also show a weaker broad absorption band at shorter wavelength ($\lambda = 450$ nm), due to $S_0–S_n$ ($n \geq 2$) transitions. Moreover, the HHBWabs increases from 28/27 nm for **1a** and **2a** to 45/42 nm for **1b** and **2b**, respectively, which suggests that a larger number of rotamers are present in the ground state for the styryl derivatives.

Emission studies show defined mirror spectra for all compounds. As expected, the addition of styryl groups in **1b** and **2b** extends delocalization of the π system, producing a redshift ($\lambda \approx 100$ nm) in their absorption and emission maxima.[24] Fluorescence quantum yields (Φ_F) of the synthesized fluorinated BODIPYs are low; this is likely to be due to intersystem crossing to triplet states induced by the iodine atoms in the 2,6-positions of the pyrrole ring.[25] The observed small Stokes shifts ($\Delta\nu$) suggest that self-absorption may also occur due to partial overlap between absorption and emission spectra. However, the measured quantum yields for all compounds are comparable to those reported in the literature for analogous non-fluorinated dyes,[22,25,26] reaching a maximum value of $\Phi_F \geq 0.2$ for styryl derivatives **1b** and **2b**. As a consequence, the multiexponential fitting of the fluorescence decay gives a similar average lifetime, τ, of about 1 ns for **1a** and **2a**, and higher values (1.4–1.7 ns) for **1b** and **2b**, with similar radiative (k_{rad}) and nonradiative (k_{nr}) constants inside the derivatives of each family. From the collected data, it seems that the insertion of branched fluorinated residues does not affect the overall optical performance of pristine dyes **6** and **7**, regardless of their number and position.

The NMR spectroscopy properties of the obtained fluorinated BODIPYs in solution were also studied. As expected, ^{19}F NMR spectra of all compounds show a single, sharp, and intense resonance at $\delta = -71$ ppm, which was related to the ^{19}F atoms of the branched fluoroalkoxy chains. Relaxivity properties of the ^{19}F nuclei were also measured (Table 1), and showed values in accordance with those of fluorinated label agents with very long T_2 values, which are desirable for ^{19}F-MRI.

Characterization in the solid state

Crystallographic studies were performed by means of single-crystal and powder XRD. All compounds were crystallized through slow evaporation of their solutions in organic solvents: **1a** from THF and **1b**, **2a**, and **2b** from acetone. The obtained crystals were poorly diffracting, very thin, almost bidimensional, with some signs of lamellar twinning. Low-temperature data collections showed poorer diffraction patterns, possibly due to a phase transition; thus data for the samples were acquired at 298 K (see Section S3 in the Supporting Information for crystallographic details).

Compounds **1a** and **1b** crystallized in the triclinic space group $P\bar{1}$, with a single molecule of the fluorinated dye in the asymmetric unit (Figure 3, *i*). Both samples share strong struc-
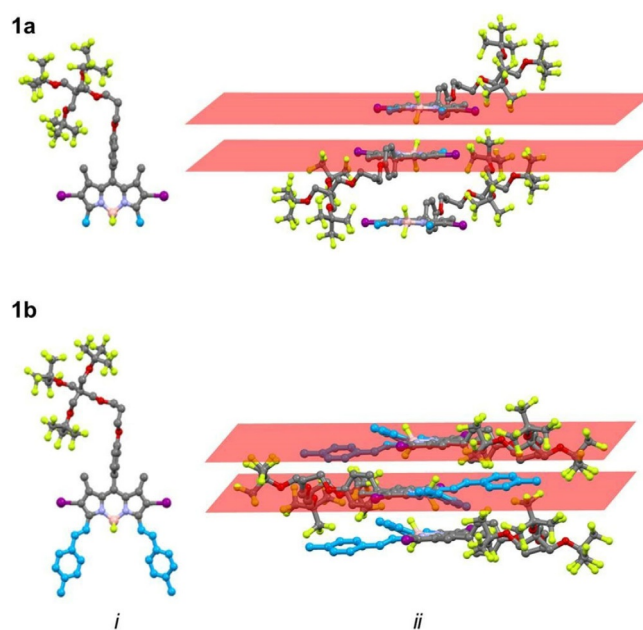

Figure 3. Crystal structures of compounds **1a** and **1b**, showing asymmetric units (*i*) and overlapping parallel π surfaces (*ii*; red planes). The distance between the red planes is 3.88 Å for **1a** and 3.92 Å for **1b**. For clarity, hydrogen atoms are omitted and substituents in positions 3 and 5 are represented in light blue. Color code: carbon (gray), nitrogen (violet), oxygen (red), boron (pink), fluorine (yellow).

tural similarities: 1) the BODIPY cores adopt a planar arrangement to create pillar architectures, 2) phenyl rings with the fluorinated unit are orthogonal to the boraindacene plane, and 3) the fluoroalkoxy chains are folded along the same direction of the BODIPY plane (Figure 3). The high fluorine content (i.e., 29 fluorine atoms) promotes segregation between the fluorocarbon and hydrocarbon regions, with the fluorinated units interacting through weak F···F contacts. From a crystallographic point of view, the perfluorinated *tert*-butyl moieties are very disordered (all of them show high atomic displacement parameters) and their detailed description is very challenging at RT. This phenomenon is very common in highly fluorinated molecules and determines the weak diffraction of these samples (Figure S2 in the Supporting Information).

In **1a** and **1b**, the aromatic plane described by the BODIPY cores adopts a parallel-displaced arrangement, in which the fluorinated tails are placed on opposite sides of the adjacent molecules. The pairing between two nearby boraindacene units is stabilized by the presence of C···F intermolecular interactions. Specifically, a C···F contact occurs between a fluorine atom of the $-BF_2$ group and a carbon atom belonging to the facing BODIPY system (C6···F2 3.10 Å for **1a** and C4···F2 3.08 Å for **1b**; Figure S3 in the Supporting Information). In addition, F···F contacts involving adjacent units of molecules of **1a** favor the parallel orientation of boraindacene planes. This interaction takes place between a fluorine atom of the $-BF_2$ group and the fluorine atom belonging to a $-CF_3$ group of a second molecule (F1···F6 2.87 Å).

The interplane distances between stacked boraindacene units are quite short, with values of 3.88 and 3.97 Å in **1a** and

3.92 and 3.99 Å **1 b** (Figure 3). The relatively larger mean value between the BODIPY cores in **1 b** can be attributed to the presence of bulky styryl substituents, which adopt a non-coplanar orientation, with respect to the heterocyclic units. Although in **1 b** the BODIPY core interplane distance is larger, the offset between the aromatic units is shorter than that in **1 a**, namely, the overlapping surface between the π systems is greater (offset distance between calculated centroids in the BODIPY units: 4.68 Å in **1 a** and 4.46 Å in **1 b**).

In addition to the F⋯F interactions stabilizing crystal packing, it is worth mentioning the contribution of halogen bonding, which occurs between the electrophilic region (σ hole) of an iodine atom and the phenoxy oxygen of a nearby molecule in **1 b** (I1⋯O1 distance 3.275 Å, 6 % reduction of the sum of the van der Waals radii, C—I⋯O angle 171.77°; Figure S4 in the Supporting Information).

Overall, the stacking and packing arrangement of BODIPY cores suggest that **1 a** and **1 b** may show a similar and low optical response, although some small structural differences are present. Indeed, it is known that the arrangement of BODIPY cores is related to the optical properties of these materials.[27] In this regard, in 2009, Akkaya et al. proposed a strategic placement of bulky functional groups on the BODIPY core to hinder the π–π stacking of the π-fluorophores, and thus, avoid emission quenching in the solid state.[27] On the other hand, it seems that an additional bulky fluorinated arm in the structure strongly affects the overall crystal packing for **2 a** and **2 b**, even if some common structural features with monofunctionalized moieties are observed, such as strong segregation among hydrocarbon/fluorocarbon units and the orthogonality of the *meso*-aryl group with respect to the boron–indacene plane.

In fact, compound **2 a** crystallized in the orthorhombic *Pbca* space group, whereas **2 b** crystallized in the triclinic space group *P*1̄, both had a single fluorinated dye molecule in the asymmetric unit (Figure 4). In **2 a**, the fluorinated alkoxy chains are almost symmetrical to the BODIPY plane and this creates isolated monolayers of aromatic units sandwiched between two fluorinated regions, with complete absence of π stacking (Figure S5 in the Supporting Information). The aromatic monolayers are assembled by a network of weak C⋯H, H⋯H, and O⋯H contacts. Specifically, an oxygen atom of the B-alkoxyl group interacts with a methyl substituent of the mesitylene ring (O6⋯H16A 2.71 Å), whereas a C⋯H contact occurs between two methyl groups on the heterocycles of two adjacent molecules (C20⋯H22A 2.78 Å).

Differently, in compound **2 b**, the fluoroalkoxy chains are not symmetrical: one of them is folded along the same direction as the styryl substituents, whereas the other one is almost linear and perpendicular to the heterocyclic plane (Figure S5 in the Supporting Information). This arrangement generates a partial overlap between π systems, owing to the C—H⋯π interaction occurring between a methyl group of the mesitylene ring and the carbon atom bonded to iodine in the BODIPY heterocycle (C1⋯H77A 2.90 Å).

The absence of BODIPY stacking in **2 a** suggests a different optical response in the solid state compared with that of **1 a** and **1 b**; hence a higher quantum yield is expected. In **2 b**, the
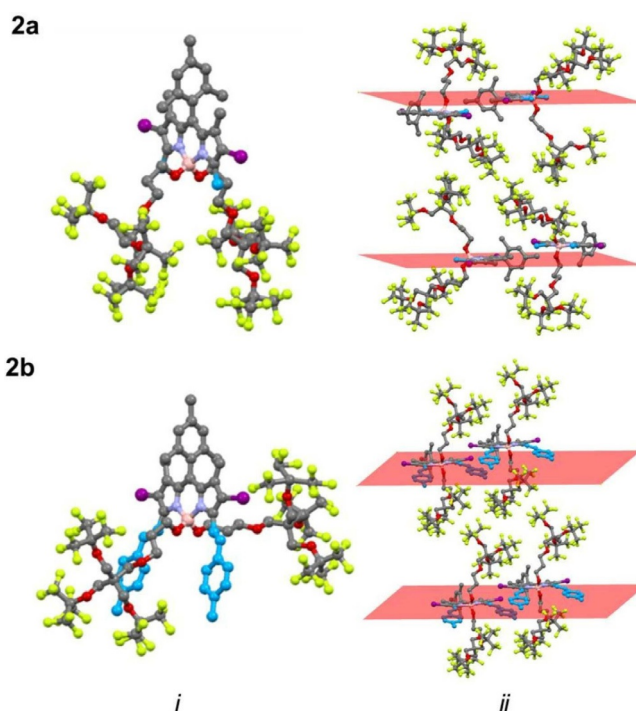

Figure 4. Crystal structures of compounds **2 a** and **2 b**, showing asymmetric units (*i*) and overlapping parallel π surfaces (*ii*; red planes). The distance between the red planes is 20.2 Å for **2 a** and 20.1 Å for **2 b**. For clarity, hydrogen atoms are omitted and substituents in positions 3 and 5 are represented in light blue. The color code is the same as that used in Figure 3.

simultaneous presence of a greater separation distance between boraindacene units and weak interactions between aromatic groups may result in a higher quantum yield than those of **1 a** and **1 b**, but lower than that of **2 a**. Notably, the good agreement between the simulated powder XRD pattern from a single-crystal experiment for the fluorinated systems and an experimental powder XRD pattern for bulk polycrystalline samples proved that the structures of **1 a**, **1 b**, **2 a**, and **2 b** obtained from single-crystal XRD data were fully representative of the bulk polycrystalline sample (Figures S6–S9 in the Supporting Information).

Optical properties in the bulk

Absorption and emission spectra of the solid compounds were recorded on bulk polycrystalline samples (Figure 5, Table 2, and Figure S1 in the Supporting Information). Absorption spectra in the solid state of both **1 a** and **2 a** reveal a defined band at $\lambda \approx 540$ nm and a small shoulder close to $\lambda = 500$ nm, similar to those obtained in THF, except for a slight redshift of about 13–12 nm (Figure 5). Absorption maxima of compounds **1 b** and **2 b** (at $\lambda = 657$ and 642 nm, respectively) are redshifted by 11 and 2 nm, respectively, compared with their absorption maxima in THF (Figure 5). The fluorescence maxima of **1 a** and **2 a**, at $\lambda = 622$ and 589 nm, respectively, are redshifted by 72 and 38 nm, respectively, in comparison with the emission maxima in THF, whereas the fluorescence maxima of compounds **1 b** and **2 b** are located at $\lambda = 807$ and 765 nm, respec-
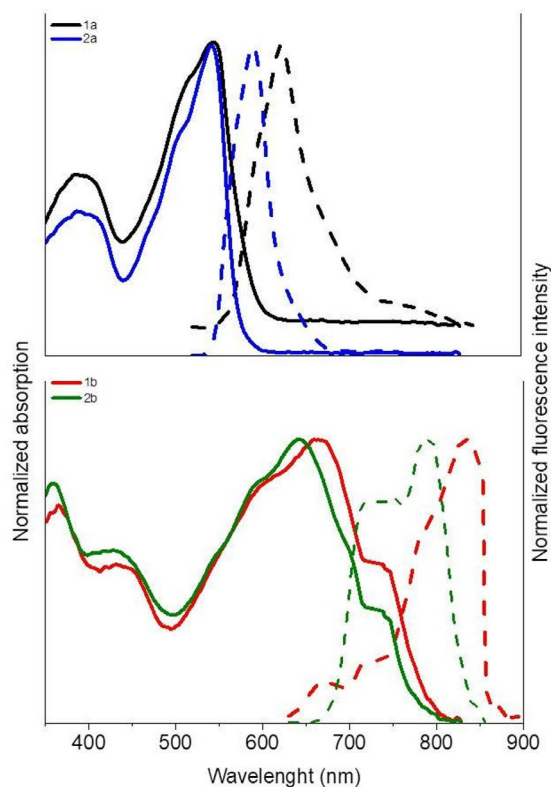
Figure 5. Solid-state absorption (solid line) and emission (dashed line) spectra of **1 a** (black), **2 a** (blue), **1 b** (red), and **2 b** (green).

Table 2. Optical properties in the solid state for the powdered dyes.

Dye	λ_{max} abs [nm]	Redshift [nm][a]	λ_{max} em [nm]	Redshift [nm][a]	Φ_F [%]
6	535	4	643	92	0.03
7	687	42	827	170	0.04
1 a	544	13	622	72	0.07
1 b	657	12	807	150	0.02
2 a	542	11	589	38	1.10
2 b	642	2	765	112	0.46

[a] Compared with the corresponding λ_{max} value in THF.

tively with a redshift of 150–112 nm compared with that in THF. In this regard, it has been reported that substituted BODIPY systems can form either J- or H-type aggregates, according to different supramolecular organizations.[28] Generally, the H aggregates result from π–π stacking of two BODIPY cores with almost parallel $S_0 \rightarrow S_1$ transition dipoles and antiparallel electrical dipole moments. This arrangement gives rise to hypochromic absorption relative to the monomer and practically no fluorescence. The J aggregates, on the contrary, present a redshifted absorption and fluorescence associated with the transition dipoles of the monomeric dyes, which are aligned in a coplanar inclined fashion, with a slip angle of <55°. For our samples, any sort of H-type exciton coupling might take place, considering the strong quenching of emission in the solid state and the observed slip angles of >64° (see the Supporting Information), which lie in the range of H

aggregates. Because the single-crystal XRD structures are fully representative of the bulk polycrystalline samples, the obtained fluorescence quantum yields are quite low. Nevertheless, a great enhancement is observed upon comparing **2 a** and **2 b** with the corresponding less fluorinated molecules **1 a** and **1 b**.

This is in agreement with the increase in stacking distance observed in the crystal structure, which decreases the well-known effect called aggregation-caused quenching (ACQ). A self-quenching effect due to spectral overlap between absorption and emission spectra, observable in Figure 5, cannot be ruled out, neither can excimer formation. Aggregation spectroscopic analysis and theoretical studies are in progress to further discuss the results obtained for optical studies on powders. Nevertheless, it is worth noting that chemical modulation of the BODIPYs can tune their emission colors from orange (**2 a**) to red (**1 a**), as quantitatively determined from the chromaticity diagram (Figure 6). Indeed, according to the CIE coordinates, the emission of these compounds lies very close to the border of the chromaticity diagram corresponding to pure colors, which is an important parameter for applications as staining dyes.
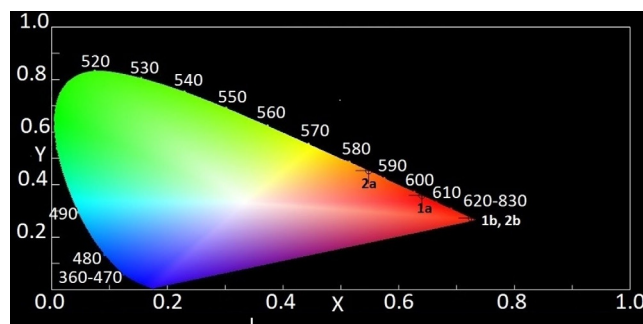

Figure 6. Chromaticity diagram (CIE 1931) for the four fluorinated BODIPY powders.

Conclusion

A small series of BODIPY dyes functionalized with multi-branched highly fluorinated groups were synthesized and characterized. The synthetic design and strategy aimed to introduce a significant number of magnetically equivalent ^{19}F atoms into the BODIPY core, without compromising the overall optical performance of the original dyes. In particular, the replacement of fluorine atoms on the boron atom provided an effective way to introduce highly fluorinated moieties onto the BODIPY core for further exploitation in the preparation of fluorescent fluorophilic materials.

Fluorinated BODIPYs **1 a,b** and **2 a,b** all showed sharp absorptions and mirror-like emission profiles in solution, similar to those of non-fluorinated homologues: for compounds **1 b** and **2 b**, modification of the BODIPY cores with styryl groups increased delocalization of the π electrons, and consequently extended the emission towards the far-red region. In BODIPYs **1 a,b** and **2 a,b**, functionalization with branched perfluoroalkoxy residues did not substantially affect the photophysical pa-

rameters, which were consistent with those of the pristine BODIPYs **6** and **7**, in terms of quantum yields, k_{rad}, and k_{nr}. Moreover, evidence of a strong, single signal in the ^{19}F NMR spectra, together with relaxivity values in agreement with those of common fluorinated probes, make these molecules good candidates as potential dual-imaging probes for FLI and ^{19}F-MRI applications.

Crystallographic investigations by means of single-crystal and powder XRD of the fluorinated dyes showed a clear separation between aromatic BODIPY cores and fluorous domains. In monosubstituted derivatives **1a** and **1b**, this gave rise to quite short interplane distances between stacked BODIPY units. On the contrary, the presence of two bulky fluorinated residues notably enhanced the segregation of boraindacene units in BODIPYs **2a** and **2b**, resulting in complete absence of π stacking. Despite the generally low values of Φ_F for all derivatives, due to the presence of iodine atoms, this structural difference was confirmed by photophysical data recorded in the solid state, which showed one order of magnitude higher Φ_F for disubstituted BODIPYs **2a** and **2b** compared with those of monosubstituted derivatives **1a** and **1b** and non-fluorinated BODIPYs **6** and **7**.

Experimental Section

General

All available chemicals and solvents were purchased from commercial sources and used without any further purification. Compounds **5**, **6**, *R*~f~-OH, and *R*~f~-Oms were prepared according to procedures reported previously in the literature (Scheme S1-2 in the Supporting Information).[19,21,29] TLC was conducted on plates precoated with silica gel Si 60-F254 (Merck, Darmstadt, Germany). Gravimetric column chromatography was carried out by using silica gel Si 60, 230–400 mesh, 0.040–0.063 mm (Merck, Darmstadt, Germany). Flash chromatography was carried out on J. T. Baker silica gel mesh size 230–400. ^{1}H and heteronuclear NMR spectra were recorded at (300 ± 3) K on a Bruker Avance III 400 MHz spectrometer equipped with a 5 mm QNP probe (^{19}F–^{31}P–^{13}C/^{1}H); chemical shifts are reported in ppm downfield from SiMe$_4$, with the residual proton (CHCl$_3$: $\delta = 7.26$ ppm, THF: $\delta = 1.73$ ppm) and carbon (CDCl$_3$: $\delta = 77.0$ ppm, THF: $\delta = 25.37$ ppm) solvent resonances as internal references. Proton and carbon assignments were achieved by means of ^{13}C-APT, ^{1}H–^{1}H COSY, and ^{1}H–^{13}C HSQC and HMBC experiments. Coupling constant values, J, are given in Hz. Mass analyses were performed on a VG Autospec M246 (Fisons) spectrometer with EBE geometry, equipped with EI and FAB sources. Absorption spectra were acquired in different solvents at room temperature on a V-630 double-beam Jasco spectrophotometer, which was equipped with halogen and deuterium lamps. Fluorescence analysis was carried out at room temperature by using a Nanolog Horiba Jobin Yvon spectrometer, equipped with a 450 W xenon short-arc excitation source. Fluorescence decays were obtained by applying time-correlated single photon counting (TCSPC) in spectroscopic grade THF on a Tempro Horiba instrument with a $\lambda = 510$ or 560 nm nano-light-emitting diode (nanoLED). A 0.01% suspension of Ludox AS40 (Aldrich) in ultrapure water was used for the prompt signal. Calibration of the equipment was realized with a solution of 4-bis(4-methyl-5-phenyl-2-oxazolyl)benzene (POPOP) in methanol (optical density 0.1 and lifetime of 0.93 ns). Data were fitted by using the software DAS6 available with the instrument. UV/Vis

spectra in the solid state were obtained in diffuse reflectance mode with a Shimadzu 2401PC spectrophotometer equipped with an integrating sphere. BaSO$_4$ pellets were used as a reference and for baseline measurements. Fluorescence spectra were recorded with a Horiba PTI Quantamaster QM-8450-22-c spectrofluorimeter, which was equipped with an integrating sphere. The excitation wavelength was chosen in agreement with solution determinations. Slits were set to maintain the linear regime of the detector. All of the spectra were corrected for background signals during measurements. Quantum yields and CIE coordinates were directly determined with the Felix software. ^{19}F T_1 and T_2 measurements were recorded at 305 K on a Bruker AV400 spectrometer operating at 400 MHz for the ^{19}F nucleus. Inversion recovery and cpmg pulse sequences were used to measure T_1 and T_2, respectively. Single-crystal X-ray structures were determined on a Bruker Kappa Apex II diffractometer at 140 K by using a fine-focus sealed Mo$_{K\alpha}$ tube, $\lambda = 0.71073$ Å. Data collection and reduction were performed by using the programs SMART and SAINT, and absorption correction, based on multiscan procedure, was achieved by using the program SADABS. Structures were solved with SHELXS-97S2 software and refined on all independent reflections by full-matrix least-squares based on $F2$ by using the SHELXL-97.S2 program. All non-hydrogen atoms were refined anisotropically. Hydrogen atoms were placed in calculated positions and refined by using a riding model. Figures were obtained with the Mercury software. Attenuated total reflectance (ATR) FTIR spectra were obtained with a Thermo Scientific Nicolet iS50 FTIR spectrometer, which was equipped with an iS50 ATR accessory (Thermo Scientific, Madison, USA). Values are given in wavenumbers rounded to 1 cm^{-1} upon automatic assignment. Melting points were also determined on a Reichert instrument, by observing the melting process through an Olympus BH-2 optical microscope.

Compound 3

4-Hydroxybenzaldehyde (0.272 g, 2.23 mmol) and 3-[3-(perfluoro-*tert*-butoxy)-2,2-bis(perfluoro-*tert*-butoxymethyl)propoxy]propyl methanesulfonate (3.1 g, 3.34 mmol) were dissolved in DMF (60 mL). Solid K$_2$CO$_3$ (0.462 g, 3,34 mmol) was added and the resulting suspension was heated at 80 °C under stirring for 16 h. The mixture was then concentrated at reduced pressure, AcOEt (100 mL) was added, and the organic phase was washed several times with water (5×20 mL). The organic phase was dried over MgSO$_4$ and the solvent was removed under reduced pressure; the residue was purified by means of gravimetric column chromatography (silica gel, petroleum ether (EtP)/AcOEt, 9:1) to give **3** as a white solid (1.84 g, 85%). ^{1}H NMR (400 MHz, CDCl$_3$): $\delta = 9.89$ (s, 1H; Ph-CHO), 7.83 (d, ^3J(H,H) = 8.3 Hz, 2H; Ph-2,6H), 6.97 (d, ^3J(H,H) = 8.3 Hz, 2H; Ph-3,5H), 4.08 (t, ^3J(H,H) = 6.5 Hz, 2H; Pr-1H), 4.03 (s, 6H; FPET-3,4,5H), 3.59 (t, ^3J(H,H) = 6.5 Hz, 2H; Pr-3H), 3.40 (s, 2H; FPET-1H), 2.07 ppm (quint, ^3J(H,H) = 6.5 Hz, 2H; Pr-2H); ^{13}C NMR (101 MHz, CDCl$_3$): $\delta = 190.9$ (Ph-CHO), 164.0 (Ph-4C), 132.1 (Ph-2,6C), 130.2 (Ph-1C), 120.3 (q, ^1J(C,F) = 292.4 Hz, FtBu-CF$_3$), 114.7 (Ph-3,5C), 79.6 (m, ^2J(C,F) = 30.2 Hz, FtBu-1C), 68.0 (Pr-3C), 66.0 (FPET-1C), 65.4 (FPET-3,4,5C), 65.0 (Pr-1C), 46.4 (FPET-2C), 29.4 ppm (Pr-2C); HRMS (EI): *m/z* calcd for C$_{27}$H$_{19}$O$_6$ [*M*]$^+$: 952.0829; found: 952.0730.

Compound 4

A solution of 2,4-dimethyl-1*H*-pyrrole (0.5 mL, 4.86 mmol) and aldehyde **3** (1.78 g, 1.87 mmol) in CH$_2$Cl$_2$ (250 mL, stabilized on amylene) was prepared under a nitrogen atmosphere. Trifluoroacetic acid (16 μL, 0.24 mmol) was added at room temperature for 2 h in

the dark. The resulting dark reddish solution was cooled at 0 °C and 2,3-dichloro-5,6-dicyano-p-benzoquinone (1.07 g, 4.71 mmol) was added as a solid in one portion. The dark solution was kept at 0 °C for 10 min. After this time, triethylamine (3.6 mL) and then boron trifluoride diethyl etherate (3.6 mL) were added. The cold bath was removed and the dark mixture was left under stirring at RT for 2 h. Water (150 mL) was added and the biphasic mixture was filtered through Celite. The organic phase was washed twice with water (100 mL each), dried over MgSO$_4$, and the solvent was removed slowly under reduced pressure. The residue was purified by means of gravimetric column chromatography (silica gel, EtP/AcOEt, 9:1) to give **4** as a dark orange solid (1.05 g, 48%). ^{1}H NMR (400 MHz, CDCl$_3$): $\delta = 7.16$ (d, $^3J(H,H) = 8.6$ Hz, 2H; Ph-2,6H), 6.97 (d, $^3J(H,H) = 8.7$ Hz, 2H; Ph-3,5H), 5.97 (s, 2H; BDP-2,6H), 4.08–4.00 (m, 8H; Pr-1H; FPET-3,4,5H), 3.62 (t, $^3J(H,H) = 6.1$ Hz, 2H; Pr-3H), 3.41 (s, 2H; FPET-1H), 2.55 (s, 6H; BDP-3,5CH$_3$), 2.08 (quint, $^3J(H,H) = 5.8$ Hz, 2H; Pr-2H), 1.42 ppm (s, 6H; BDP-1,7CH$_3$); ^{13}C NMR (101 MHz, CDCl$_3$): $\delta = 159.5$ (Ph-4C), 155.3 (BDP-3,5C), 143.2 (BDP-9,10C), 141.9 (BDP-8C), 131.9 (BDP-1,7C), 129.3 (Ph-2,6C), 127.2 (Ph-1C), 120.2 (q, $^1J(C,F) = 291.8$ Hz, FtBu-CF$_3$), 114.9 (Ph-3,5C), 80.8–75.7 (m, FtBu-1C), 68.1 (Pr-3C), 65.8 (FPET-1C), 65.2 (FPET-3,4,5C), 64.5 (Pr-1C), 46.3 (FPET-2C), 29.4 (Pr-2C), 14.6 (BDP-3,5CH$_3$), 14.5 ppm (BDP-1,7CH$_3$); ^{19}F NMR (377 MHz, CDCl$_3$): $\delta = -71.39$ (s), -147.33 ppm (q, $^1J(B,F) = 32.8$ Hz); MS (FAB): m/z: 1170 [M]$^+$.

Compound 1 a

BODIPY **4** (0.50 g, 0.43 mmol) was suspended in EtOH (85 mL). Solid iodic acid (0.151 g, 0.86 mmol) and iodine (0.272 g, 1.08 mmol) were added, and then the mixture was warmed at 60 °C under stirring. The reaction was followed by TLC (EtP/AcOEt 9:1) until the starting material completely disappeared (about 1 h). The solvent was removed by evaporation under reduced pressure; the residue was dissolved in AcOEt (100 mL) and washed with a saturated aqueous solution of sodium thiosulfate (2×50 mL) and water (2×50 mL). After evaporation of the organic phase, which had been dried over MgSO$_4$, the solid residue was purified by means of precipitation from a mixture of THF/MeOH (1 mL/150 mL) to afford **1 a** as a bright orange solid (0.53 g, 87%). M.p. 160 °C; FTIR-ATR: $\nu = 1606$ (C=C$_{Ar}$), 1530 (B-F), 1346 (C-N), 1252 (C-O), 1184–1154 (C=C$_{Ar}$), 1117–971 (C-H$_{Ar}$), 737–726 (C-F), 590–526 cm^{-1} (C-I); ^{1}H NMR (400 MHz, [D$_8$]THF): $\delta = 7.25$ (d, $^3J(H,H) = 8.6$ Hz, 2H; Ph-2,6H), 7.11 (d, $^3J(H,H) = 8.6$ Hz, 2H; Ph-3,5H), 4.14 (d, $^3J(H,H) = 6.7$ Hz, 8H; Pr-1H; FPET-3,4,5H), 3.66 (t, $^3J(H,H) = 6.3$ Hz, 2H; Pr-3H), 3.46 (s, 2H,FPET-1H), 2.59 (s, 6H; BDP-3,5CH$_3$), 2.10 (quint, $^3J(H,H) = 6.2$ Hz, 2H; Pr-2H), 1.47 ppm (s, 6H; BDP-1,7CH$_3$); ^{13}C NMR (101 MHz, [D$_8$]THF): $\delta = 161.2$ (Ph-4C), 157.2 (BDP-3,5C), 145.9 (BDP-9,10C), 143.1 (BDP-8C), 132.7 (BDP-1,7C), 130.3 (Ph-2,6C), 127.7 (Ph-1C), 121.4 (q, $^1J(C,F) = 291.8$ Hz, FtBu-CF$_3$), 116.1 (Ph-3,5C), 85.8 (BDP-2,6C), 81.1–80.8 (m, FtBu-1C), 69.0 (Pr-3C), 66.2 (FPET-1C, FPET-3,4,5C), 65.5 (Pr-1C), 47.4 (FPET-2C), 30.4 (Pr-2C), 17.4 (BDP-1,7CH$_3$), 16.1 ppm (BDP-3,5CH$_3$); ^{19}F NMR (377 MHz, [D$_8$]THF) $\delta = -73.91$, -149.18 ppm (q, $^1J(B,F) = 31.7$ Hz); MS (FAB): m/z: 1422 [M]$^+$.

Compound 1 b

BODIPY **1 a** (0.25 g, 0.176 mmol) was suspended in dry CH$_3$CN (30 mL) before p-tolualdehyde (0.21 mL, 1.78 mmol), molecular sieves (union carbide type 4 Å; 3.0 g), glacial AcOH (0.12 mL, 2.14 mmol), and pyrrolidine (0.18 mL, 2.14 mmol) were added. This mixture was stirred in a thermostated bath at 115°. The solution changed color in about 15–20 min, from deep purple to dark purple. The reaction was followed by TLC (EtP/AcOEt 9:1); after

1 h, aliquots of glacial AcOH (0.12 mL, 2.14 mmol) and pyrrolidine (0.18 mL, 2.14 mmol) were added. Complete disappearance of the starting material was achieved after 1 h. The mixture was then cooled at room temperature and filtered through a sintered septum; the sieves were washed with Et$_2$O until a colorless filtrate was obtained. Evaporation of the solvents under reduced pressure gave a dark residue that was purified by means of gravimetric column chromatography (silica gel); first eluted with EtP/AcOEt 9:1 and then with EtP/CH$_2$Cl$_2$ 8:2 to collect the dark green fraction. The dark bluish green solid collected after evaporation of the solvent was treated with boiling methanol (100 mL) to give **1 b** as a copper colored solid (0.142 g, 49%). M.p. 163 °C; ^{1}H NMR (400 MHz, [D$_8$]THF): $\delta = 8.21$ (d, $^3J(H,H) = 16.7$ Hz, 2H; Styr-2H), 7.72 (d, $^3J(H,H) = 16.7$ Hz, 2H; Styr-1H), 7.54 (d, $^3J(H,H) = 8.1$ Hz, 4H; Ph(B)-2,6H), 7.30 (d, $^3J(H,H) = 8.6$ Hz, 2H; Ph(A)-2,6H), 7.24 (d, $^3J(H,H) = 8.1$ Hz, 4H; Ph(B)-3,5H), 7.13 (d, $^3J(H,H) = 8.6$ Hz, 2H; Ph(A)-3,5H), 4.21–4.10 (m, 8H; FPET-3,4,5H; Pr-1H), 3.68 (t, $^3J(H,H) = 6.3$ Hz, 2H; Pr-3H), 3.47 (s, 2H; FPET-1H), 2.38 (s, 6H; Ph(B)-4CH$_3$), 2.12 (quint, $^3J(H,H) = 6.2$ Hz, 2H; Pr-2H), 1.55 ppm (s, 6H; BDP-1,7CH$_3$); ^{13}C NMR (101 MHz, [D$_8$]THF): $\delta = 161.3$ (Ph(A)-4C), 151.3 (BDP-3,5C), 146.7 (BDP-9,10C), 140.8 (BDP-8C), 140.4 (Ph(B)-4C), 140.0 (Styr-2C), 135.1 (Ph(B)-1C), 134.3 (BDP-1,7C), 130.8 (Ph(A)-2,6C), 130.4 (Ph(B)-3,5C), 128.3 (Ph(B)-2,6C), 128.2 (Ph(A)-1C), 121.4 (q, $^1J(C,F) = 291.6$ Hz, FtBu-CF$_3$), 119.0 (Styr-1C), 116.1 (Ph(A)-3,5C), 83.1 (BDP-2,6C), 80.5 (m, FtBu-1C), 69.0 (Pr-3C), 66.1 (FPET-3,4,5C), 65.5 (FPET-1C), 47.4 (FPET-2C), 30.4 (Pr-2C), 21.50 (Ph(B)-4CH$_3$), 18.0 ppm (BDP-1,7CH$_3$); ^{19}F NMR (377 MHz, [D$_8$]THF): $\delta = -72.03$ (s), -139.97 ppm (q, $^1J(B,F) = 33.7$ Hz); FTIR-ATR: $\nu = 1622$–1606 (C=C$_{Ar}$), 1512 (B-F), 1468–1353 (C-N), 1245 (C-O), 1186–1157 (C=C$_{Ar}$), 1101–972 (C-H$_{Ar}$), 737–726 (C-F), 574–538 cm^{-1} (C-I); MS (FAB): m/z: 1626 [M]$^+$.

Compound 5

A solution of 2,4-dimethyl-1H-pyrrole (2 mL, 19.4 mmol) and 2,4,6-trimethylbenzaldehyde (1.1 mL, 7.46 mmol) in CH$_2$Cl$_2$ (500 mL, stabilized on amylene) was prepared under a nitrogen atmosphere. Trifluoroacetic acid (74 μL, 0.97 mmol) was added at room temperature and the mixture was stirred at room temperature for 3 h in the dark. The resulting dark reddish solution was cooled at 0 °C and 2,3-dichloro-5,6-dicyano-p-benzoquinone (4.40 g, 19.4 mmol) was added as a solid in one portion. The dark red solution was kept at 0 °C for 10 min. After this time, triethylamine (15 mL) and then boron trifluoride diethyl etherate (15 mL) were added. The cold bath was removed and the dark mixture was left under stirring for 2 h. Water (200 mL) was added and the biphasic mixture was filtered through Celite. The organic phase was washed a few times with water (3×300 mL), dried over MgSO$_4$, and the solvent was removed under reduced pressure. The residue was purified by means of gravimetric column chromatography (silica gel, CH$_2$Cl$_2$) to afford **5** as a bright red solid (2.43 g, 89%). ^{1}H NMR (400 MHz, CDCl$_3$): $\delta = 6.94$ (s, 2H; Mes-3,5H), 5.96 (s, 2H; BDP-2,6H), 2.56 (s, 6H; BDP-3,5CH$_3$), 2.33 (s, 3H; Mes-4CH$_3$), 2.09 (s, 6H; Mes-2,6CH$_3$), 1.38 ppm (s, 6H; BDP-1,7CH$_3$); ^{13}C NMR (101 MHz, CDCl$_3$): $\delta = 155.1$ (BDP-3,5C), 142.3 (BDP-9,10C), 141.7 (BDP-8C), 138.6 (Mes-4C), 134.9 (Mes-2,6C), 131.1 (Mes-1C), 130.6 (BDP-1,7C), 129.0 (Mes-3,5C), 120.8 (BDP-2,6C), 21.2 (Mes-4CH$_3$), 19.5 (Mes-2,6CH$_3$), 14.7 (BDP-3,5CH$_3$), 13.4 ppm (BDP-1,7CH$_3$); ^{19}F NMR (377 MHz, CDCl$_3$): $\delta = -145.84$ ppm (q, $^1J(B,F) = 32.1$ Hz); HRMS (EI): m/z calcd for C$_{22}$H$_{25}$BF$_2$N$_2$ [M]$^+$: 366.2079; found: 366.2072.

Compound 6

BODIPY **5** (1.0 g, 2.73 mmol) was dissolved in EtOH (400 mL) before iodic acid (1 g, 5.68 mmol) and iodine (1.8 g, 7.09 mmol) were added and the mixture was warmed at 60 °C under stirring. The re-

action was followed by TLC (EtP/CH$_2$Cl$_2$ 1:1) until the starting material completely disappeared (about 1 h). The mixture was concentrated by evaporation under reduced pressure; the residue was dissolved in AcOEt (150 mL) and washed with a saturated aqueous solution of sodium thiosulfate (2×50 mL) and water (2×50 mL). After evaporation of the organic phase, which was dried over MgSO$_4$, the solid residue was purified by means of gravimetric column chromatography (silica gel, EtP/CH$_2$Cl$_2$, 1:1) to afford **6** as a dark red solid (1.47 g, 93%). M.p. 219°C; FTIR-ATR: ν = 2917 (-CH$_2$), 1521 (B-F), 1455 (B-N), 1340–1309 (C-N), 1177–1117(C=C$_{Ar}$), 1080 (C-H$_{Ar}$), 994–914 (C=C), 587–524 cm^{-1} (C-I); ^{1}H NMR (400 MHz, CDCl$_3$): δ = 6.97 (s, 2H; Mes-3,5H), 2.65 (s, 6H; BDP-3,5CH), 2.36 (s, 3H; Mes-4CH$_3$), 2.06 (s, 6H; Mes-2,6CH$_3$), 1.40 ppm (s, 6H; BDP-1,7CH$_3$); ^{13}C NMR (101 MHz, CDCl$_3$): δ = 156.4 (BDP-3,5C), 144.6 (BDP-9,10C), 141.7 (BDP-8C), 139.3 (Mes-4C), 134.8 (Mes-2,6C), 130.9 (Mes-1C), 130.5 (BDP-1,7C), 129.3 (Mes-3,5C), 85.3 (BDP-2,6C), 21.3 (Mes-4CH$_3$), 19.5 (Mes-2,6CH$_3$), 16.1 (BDP-3,5CH$_3$), 15.8 ppm (BDP-1,7CH$_3$); ^{19}F NMR (377 MHz, CDCl$_3$): δ = −145.84 ppm (q, ^1J(B,F) = 32.1 Hz); HRMS (EI): *m/z* calcd for C$_{22}$H$_{23}$BF$_2$I$_2$N$_2$ [*M*]$^+$: 618.0012; found: 618.0020.

Compound 2a

BODIPY **6** (0.120 g, 0.194 mmol) was dissolved in dry CH$_2$Cl$_2$ (12 mL) at 50°C before solid AlCl$_3$ (77 mg, 0.582 mmol) was added and the mixture was stirred at 50°C for 5 min. The violet–blue solution was then cooled at room temperature before a solution of 3-[3-(*tert*-butoxy)-2,2-bis(*tert*-butoxymethyl)propoxy]propan-1-ol (0.820 g, 0.967 mmol) in a mixture of CH$_2$Cl$_2$ (10 mL) and the minimum amount of Et$_2$O (1 mL) was added dropwise. The reaction was followed by TLC (EtP/AcOEt 98:2). After 2 h at room temperature, the starting material was still present, so the mixture was then warmed at 50°C for another hour. After this time, the starting material had completely disappeared. The solvents were removed by evaporation under reduced pressure; the solid residue was purified by means of gravimetric column chromatography (silica gel, EtP/THF, 100:1 to 100:2) to afford **2a** as a dark red solid (0.287 g, 65%). M.p. 166°C; ^{1}H NMR (400 MHz, [D$_8$]THF): δ = 7.07 (s, 2H; Mes-3,5H), 4.10 (s, 12H; FPET-3,4,5H), 3.50 (t, ^3J(H,H) = 7.1 Hz, 4H; Pr-3H), 3.38 (s, 4H; FPET-1H), 2.99 (t, ^3J(H,H) = 6.0 Hz, 4H; Pr-1H), 2.62 (s, 6H; BDP-3,5CH$_3$), 2.36 (s, 3H; Mes-4CH$_3$), 2.05 (s, 6H; Mes-2,6CH$_3$), 1.63 (quint, ^3J(H,H) = 6.6 Hz, 4H; Pr-2H), 1.42 ppm (s, 6H; BDP-1,7CH$_3$); ^{13}C NMR (101 MHz, [D$_8$]THF): δ = 157.0 (BDP-3,5C), 143.7 (BDP-9,10C), 142.2 (BDP-8C), 140.3 (Mes-4C), 135.6 (Mes-2,6C), 132.8 (BDP-1,7C), 132.6 (Mes-1C), 130.2 (Mes-3,5C), 121.3 (q, ^1J(C,F) = 292.4 Hz, F*t*Bu-CF3), 85.6 (BDP-2,6C), 81.1–79.9 (m, F*t*Bu-1C), 70.7 (Pr-3C), 66.4 (FPET-3,4,5C), 66.1 (FPET-1C), 58.9 (Pr-1C), 47.3 (FPET-2C), 32.8 (Pr-2C), 21.3 (Mes-4CH$_3$), 19.3 (Mes-2,6CH$_3$), 16.2 (BDP-3,5CH$_3$), 16.0 ppm (BDP-1,7CH$_3$); ^{19}F NMR (377 MHz, [D$_8$]THF) δ = −73.92; FTIR-ATR: ν = 1528 (B-O), 1489 (C-N), 1247 (C-O), 1152 (C=C$_{Ar}$), 1013–971 (C-H$_{Ar}$), 737–726 (C-F), 538 cm^{-1} (C-I); MS (FAB): *m/z*: 2274 [*M*]$^+$.

Compound 7

BODIPY **6** (0.20 g, 0.32 mmol) was suspended in dry CH$_3$CN (20 mL) before *p*-tolualdehyde (0.40 mL, 3.38 mmol), molecular sieves (union carbide type 4 Å; 4.0 g), glacial AcOH (0.2 mL, 3.49 mmol), and pyrrolidine (0.3 mL, 3.59 mmol) were added. This mixture was stirred in a thermostated bath at 95°C. The solution changed color in about 15–20 min, from deep purple to dark green; TLC at this stage (EtP/CH$_2$Cl$_2$ 3:2) confirmed the absence of starting material. The mixture was cooled to room temperature and filtered through a sintered septum; the sieve was washed with CH$_2$Cl$_2$ until a colorless filtrate was obtained. Evaporation of the solvents under reduced pressure gave a dark residue that was purified by means of flash column chromatography (silica gel, EtP/CH$_2$Cl$_2$, 3:2) to give **7** as a dark green solid (0.22 g, 82%). M.p. 233°C; ^{1}H NMR (400 MHz, CDCl$_3$): δ = 8.14 (d, ^3J(H,H) = 16.7 Hz, 2H; Styr-2H), 7.67 (d, ^3J(H,H) = 16.7 Hz, 2H; Styr-1H), 7.56 (d, ^3J(H,H) = 8.1 Hz, 4H; Ph-2,6H), 7.23 (d, ^3J(H,H) = 8.1 Hz, 4H; Ph-3,5H), 6.99 (s, 2H; Mes-3,5H), 2.40 (s, 6H; Ph-4CH$_3$), 2.37 (s, 3H; Mes-4CH$_3$), 2.09 (s, 6H; Mes-2,6-CH$_3$), 1.48 ppm (s, 6H; BDP-1,7-CH$_3$); ^{13}C NMR (101 MHz, CDCl$_3$): δ = 150.4 (BDP-3,5C), 145.2 (BDP-9,10C), 139.5 (Styr-2C; Ph-4C), 139.3 (Mes-4C; BDP-8C), 135.3 (Mes-2,6C), 134.1 (Ph-1C), 132.1 (BDP-1,7C), 131.3 (Mes-1C), 129.6 (Ph-3,5C), 129.3 (Mes-3,5C), 127.7 (Ph-2,6C), 118.0 (Styr-1C), 82.6 (BDP-2,6C), 21.5 (Ph-4CH$_3$), 21.3 (Mes-4CH$_3$), 19.7 (Mes-2,6CH$_3$), 16.3 ppm (BDP-1,7CH$_3$); ^{19}F NMR (377 MHz, CDCl$_3$): δ = −139.25 ppm (q, ^1J(B,F) = 33.2 Hz); FTIR-ATR: ν = 1619–1604 (C=C$_{Styr}$), 1510 (B-F), 1456–1309 (C-N), 1168 (C=C$_{Ar}$), 1080–956 (C-H$_{Ar}$), 508 cm^{-1} (C-I); MS (EI): *m/z*: 822 [*M*]$^+$.

Compound 2b

BODIPY **7** (0.150 g, 0.182 mmol) was dissolved in dry THF (15 mL). Solid AlCl$_3$ (73 mg, 0.546 mmol) was added and the mixture was stirred at 60°C for 5 min. The dark green–blue solution was then cooled at room temperature before a solution of 3-[3-(*tert*-butoxy)-2,2-bis(*tert*-butoxymethyl)propoxy]propan-1-ol (1.3 g, 1.53 mmol) in anhydrous THF (5 mL) was added dropwise. After 1 h at room temperature, the reaction was monitored by TLC (EtP/THF 100:1), which showed the presence of the main product (R_f = 0.5) and other weak spots at lower R_f. The mixture was then warmed at 60°C for 2 h. Once cooled to room temperature, the mixture was diluted with AcOEt (30 mL) and washed with water (2×10 mL). The solvents were removed by evaporation under reduced pressure. The first dark green fraction (280 mg) was collected by flash column chromatography (silica gel, EtP/THF, 100:1) and washed with hot EtOH (25 mL) to afford **2b** as a dark green solid (0.235 g, 52%). M.p. 199°C; ^{1}H NMR (400 MHz, [D$_8$]THF): δ = 8.26–8.07 (m, 4H; Styr-1H, Styr-2H), 7.53 (d, ^3J(H,H) = 8.1 Hz, 4H; Ph-2,6H), 7.20 (d, ^3J(H,H) = 7.8 Hz, 4H; Ph-3,5H), 7.10 (s, 2H; Mes-3,5H), 3.94 (s, 12H; FPET-3,4,5H), 3.33 (t, ^3J(H,H) = 7.6 Hz, 4H; Pr-3H), 3.06 (t, ^3J(H,H) = 5.7 Hz, 4H; Pr-1H), 2.88 (s, 4H; FPET-1H), 2.41–2.31 (m, 9H; Mes-4CH$_3$, Ph-4CH$_3$), 2.10 (s, 6H; Mes-2,6CH$_3$), 1.58 (m, 4H; Pr-2H), 1.50 ppm (s, 6H; BDP-1,7CH$_3$); ^{13}C NMR (101 MHz, [D$_8$]THF): δ = 151.1 (BDP-3,5C), 144.7 (BDP-9,10C), 140.4 (Mes-4C), 140.2 (BDP-8C), 139.7 (Ph-4C), 138.3 (Styr-2C), 136.1 (Mes-2,6C), 135.7 (Ph-1C), 134.4 (BDP-1,7C), 133.0 (Mes-1C), 130.2 (Ph-3,5C, Mes-3,5C), 128.1 (Ph-2,6C), 121.3 (q, ^1J(C,F) = 292.2 Hz, F*t*Bu-CF$_3$), 120.5 (Styr-1C), 82.1 (BDP-2,6C), 80.9–80.1 (m, F*t*Bu-1C), 71.7 (Pr-3C), 65.8 (FPET-3,4,5C), 65.3 (FPET-1C), 59.0 (Pr-1C), 47.2 (FPET-2C), 32.8 (Pr-2C), 21.3 (Mes-4CH$_3$), 21.2 (Ph-4CH$_3$), 19.5 (Mes-2,6CH$_3$), 16.6 ppm (BDP-1,7CH$_3$); ^{19}F NMR (377 MHz, [D$_8$]THF): δ = −72.08 ppm; FTIR-ATR: ν = 1622 (C=C$_{Styr}$), 1510 (B-O), 1349 (C-N), 1251 (C-O), 1183–1151 (C=C$_{Ar}$), 1074–971 (C-H$_{Ar}$), 736–726 (C-F), 538 cm^{-1} (C-I); MS (FAB): *m/z*: 2478 [*M*]$^+$.

[1] a) G. Ulrich, R. Ziessel, A. Harriman, *Angew. Chem. Int. Ed.* **2008**, *47*, 1184–1201; *Angew. Chem.* **2008**, *120*, 1202–1219; b) A. Loudet, K. Burgess, *Chem. Rev.* **2007**, *107*, 4891–4932; c) E. V. de Wael, J. A. Pardoen, J. A. van Koeveringe, J. Lugtenburg, *Recl. Trav. Chim. Pays-Bas* **2010**, *96*, 306–309.

[2] N. Boens, B. Verbelen, W. Dehaen, *Eur. J. Org. Chem.* **2015**, 6577–6595.

[3] H. Klfout, A. Stewart, M. Elkhalifa, H. He, *ACS Appl. Mater. Interfaces* **2017**, *9*, 39873–39889.

[4] K. Park Sang, H. Kim Jin, Y. Park Soo, *Adv. Mater.* **2018**, *30*, 1704759.

[5] a) R. T. Grant, P. Michetti, A. J. Musser, P. Gregoire, T. Virgili, E. Vella, M. Cavazzini, K. Georgiou, F. Galeotti, C. Clark, J. Clark, C. Silva, D. G. Lidzey, *Adv. Opt. Mater.* **2016**, *4*, 1615–1623; b) O. García, R. Sastre, A. del Agua, A. Costela, I. Garcia-Moreno, F. Lopez Arbeloa, J. Banuelos Prieto, I. Lopez Arbeloa, *J. Phys. Chem. C* **2007**, *111*, 1508–1516.

[6] a) B. Bertrand, K. Passador, C. Goze, F. Denat, E. Bodio, M. Salmain, *Coord. Chem. Rev.* **2018**, *358*, 108–124; b) T. Kowada, H. Maeda, K. Kikuchi, *Chem. Soc. Rev.* **2015**, *44*, 4953–4972; c) S. Kolemen, E. U. Akkaya, *Coord. Chem. Rev.* **2018**, *354*, 121–134.

[7] a) V. Lakshmi, R. Sharma, M. M. Ravikanth, *Rep. Org. Chem.* **2015**, *6*, 1–24; b) A. B. Descalzo, H.-J. Xu, Z. Shen, K. Rurack, *J. Photochem. Photobiol. A* **2018**, *352*, 98–105; c) B. Brizet, A. Eggenspiller, C. P. Gros, J.-M. Barbe, C. Goze, F. Denat, P. D. Harvey, *J. Org. Chem.* **2012**, *77*, 3646–3650; d) N. Zhao, S. Xuan, F. R. Fronczek, K. M. Smith, M. G. H. Vicente, *J. Org. Chem.* **2017**, *82*, 3880–3885; e) C. L. Hamon, C. L. Dorsey, T. Özel, E. M. Barnes, T. W. Hudnall, T. Betancourt, *J. Nanopart. Res.* **2016**, *18*, 207; f) P. Didier, G. Ulrich, Y. Mély, R. Ziessel, *Org. Biomol. Chem.* **2009**, *7*, 3639–3642; g) S. Mula, S. Frein, V. Russo, G. Ulrich, R. Ziessel, J. Barberá, R. Deschenaux, *Chem. Mater.* **2015**, *27*, 2332–2342; h) S. Zhang, X. Liu, W. Yuan, W. Zheng, H. Li, C. Li, Y. Sun, Y. Wang, Y. Yang, Y. Li, W. Liu, *Dyes Pigm.* **2018**, *159*, 406–418; i) Y. Ni, J. Wu, *Org. Biomol. Chem.* **2014**, *12*, 3774–3791.

[8] a) L. Yao, S. Xiao, F. Dan, *J. Chem.* **2013**, *2013*, 10; b) L. C. D. Rezende, F. S. Emery, *Orbital: Electron. J. Chem.* **2013**, *5*, 62–83; c) Y. S. Marfin, A. V. Solomonov, A. S. Timin, E. V. Rumyantsev, *Curr. Med. Chem.* **2017**, *24*, 2745–2772; d) J. Zhang, B. Zhao, C. Li, X. Zhu, R. Qiao, *Sens. Actuators B* **2014**, *196*, 117–122; e) L. Fu, F.-F. Wang, T. Gao, R. Huang, H. He, F.-L. Jiang, Y. Liu, *Sens. Actuators B* **2015**, *216*, 558–562; f) H.-C. Xia, X.-H. Xu, Q.-H. Song, *Anal. Chem.* **2017**, *89*, 4192–4197; g) L.-Y. Niu, Y.-S. Guan, Y.-Z. Chen, L.-Z. Wu, C.-H. Tung, Q.-Z. Yang, *J. Am. Chem. Soc.* **2012**, *134*, 18928–18931; h) E. Okutan, S. O. Tümay, S. Yeşilot, *J. Fluoresc.* **2016**, *26*, 2333–2343; i) Y. Zhang, S. Swaminathan, S. Tang, J. Garcia-Amorós, M. Boulina, B. Captain, J. D. Baker, F. M. Raymo, *J. Am. Chem. Soc.* **2015**, *137*, 4709–4719.

[9] a) M. Ceulemans, K. Nuyts, M. W. De Borggraeve, N. T. Parac-Vogt, *Inorganics* **2015**, *3*, 519–533; b) L. Dura, M. Wächtler, S. Kupfer, J. Kübel, J. Ahrens, S. Höfler, M. Bröring, B. Dietzek, T. Beweries, *Inorganics* **2017**, *5*, 21–37; c) C. R. Anderson, J. J. Rychak, M. Backer, J. Backer, K. Ley, A. L. Klibanov, *Invest. Radiol.* **2010**, *45*, 579–585.

[10] a) S. Cherumukkil, B. Vedhanarayanan, G. Das, V. K. Praveen, A. Ajayaghosh, *Bull. Chem. Soc. Jpn.* **2018**, *91*, 100–120; b) A. V. Solomonov, Y. S. Marfin, E. V. Rumyantsev, *Dyes Pigm.* **2019**, *162*, 517–542; c) A. Sampedro, Á. Ramos-Torres, C. Schwöppe, C. Mück-Lichtenfeld, I. Helmers, A. Bort, I. Díaz-Laviada, G. Fernández, *Angew. Chem. Int. Ed.* **2018**, *57*, 17235–17239; *Angew. Chem.* **2018**, *130*, 17481–17485; d) G. Fan, Y.-X. Lin, L. Yang, F.-P. Gao, Y.-X. Zhao, Z.-Y. Qiao, Q. Zhao, Y.-S. Fan, Z. Chen, H. Wang, *Chem. Commun.* **2015**, *51*, 12447–12450.

[11] a) I. Tirotta, V. Dichiarante, C. Pigliacelli, G. Cavallo, G. Terraneo, F. B. Bombelli, P. Metrangolo, G. Resnati, *Chem. Rev.* **2015**, *115*, 1106–1129; b) S. Bo, C. Song, Y. Li, W. Yu, S. Chen, X. Zhou, Z. Yang, X. Zheng, Z.-X. Jiang, *J. Org. Chem.* **2015**, *80*, 6360–6366; c) W. Yu, Y. Yang, S. Bo, Y. Li, S. Chen, Z. Yang, X. Zheng, Z.-X. Jiang, X. Zhou, *J. Org. Chem.* **2015**, *80*, 4443–4449.

[12] A. M. Huynh, A. Mueller, S. M. Kessler, S. Henrikus, C. Hoffmann, A. K. Kiemer, A. Buecker, G. Jung, *ChemMedChem* **2016**, *11*, 1568–1575.

[13] a) A. Savoldelli, Q. Meng, R. Paolesse, F. R. Fronczek, K. M. Smith, M. G. H. Vicente, *J. Org. Chem.* **2018**, *83*, 6498–6507; b) X.-D. Jiang, T. Fang, X. Liu, D. Xi, *Eur. J. Org. Chem.* **2017**, 5074–5079; c) D. K. Kölmel, A. Hörner, J. A. Castañeda, J. A. P. Ferencz, A. Bihlmeier, M. Nieger, S. Bräse, L. A. Padilha, *J. Phys. Chem. C* **2016**, *120*, 4538–4545; d) L. Lempke, T. Fischer, J. Bell, W. Kraus, K. Rurack, N. Krause, *Org. Biomol. Chem.* **2015**, *13*, 3787–3791; e) M. Hecht, T. Fischer, P. Dietrich, W. Kraus, A. B. Descalzo, W. E. S. Unger, K. Rurack, *ChemistryOpen* **2013**, *2*, 25–38; f) G. Vives, C. Giansante, R. Bofinger, G. Raffy, A. D. Guerzo, B. Kauffmann, P. Batat, G. Jonusauskas, N. D. McClenaghan, *Chem. Commun.* **2011**, *47*, 10425–10427; g) O. Galangau, C. Dumas-Verdes, R. Meallet-Renault, G. Clavier, *Org. Biomol. Chem.* **2010**, *8*, 4546–4553.

[14] M. P. Krafft, J. G. Riess, *Curr. Opin. Colloid Interface Sci.* **2015**, *20*, 192–212.

[15] a) V. Dichiarante, M. I. Martinez Espinoza, L. Gazzera, M. Vuckovac, M. Latikka, G. Cavallo, G. Raffaini, R. Oropesa-Nuñez, C. Canale, S. Dante, S. Marras, R. Carzino, M. Prato, R. H. A. Ras, P. Metrangolo, *ACS Sustainable Chem. Eng.* **2018**, *6*, 9734–9743; b) V. Dichiarante, R. Milani, P. Metrangolo, *Green Chem.* **2018**, *20*, 13–27.

[16] S.-W. Lo, E. Law, M. Y. Lui, X.-G. Wei, K.-C. Lau, C. Y. Ma, M. B. Murphy, I. T. Horváth, *Org. Chem. Front.* **2014**, *1*, 1180–1187.

[17] C. F. A. Gómez-Durán, I. Esnal, I. Valois-Escamilla, A. Urías-Benavides, J. Bañuelos, I. López Arbeloa, I. García-Moreno, E. Peña-Cabrera, *Chem. Eur. J.* **2016**, *22*, 1048–1061.

[18] N. Epelde-Elezcano, V. Martínez-Martínez, E. Peña-Cabrera, C. F. A. Gómez-Durán, I. L. Arbeloa, S. Lacombe, *RSC Adv.* **2016**, *6*, 41991–41998.

[19] X. Yue, M. B. Taraban, L. L. Hyland, Y. B. Yu, *J. Org. Chem.* **2012**, *77*, 8879–8887.

[20] a) B. Brizet, C. Bernhard, Y. Volkova, Y. Rousselin, P. D. Harvey, C. Goze, F. Denat, *Org. Biomol. Chem.* **2013**, *11*, 7729–7737; b) C. Tahtaoui, C. Thomas, F. Rohmer, P. Klotz, G. Duportail, Y. Mély, D. Bonnet, M. Hibert, *J. Org. Chem.* **2007**, *72*, 269–272.

[21] A. B. Nepomnyashchii, M. Bröring, J. Ahrens, A. J. Bard, *J. Am. Chem. Soc.* **2011**, *133*, 8633–8645.

[22] Y. Rong, C. Wu, J. Yu, X. Zhang, F. Ye, M. Zeigler, M. E. Gallina, I. C. Wu, Y. Zhang, Y.-H. Chan, W. Sun, K. Uvdal, D. T. Chiu, *ACS Nano* **2013**, *7*, 376–384.

[23] Y. Yu, X. Yue, (2013). Dendrimers and methods of preparing same through proportionate branching. US 2013/0197271 A1, filed 29 January 2013 and issued 1 August, **2013**.

[24] a) K. Rurack, M. Kollmannsberger, J. Daub, *Angew. Chem. Int. Ed.* **2001**, *40*, 385–387; *Angew. Chem.* **2001**, *113*, 396–399; b) D. Marushchak, S. Kalinin, I. Mikhalyov, N. Gretskaya, L. B. Å. Johansson, *Spectrochim. Acta Part A* **2006**, *65*, 113–122.

[25] M. Gorbe, A. M. Costero, F. Sancenón, R. Martínez-Máñez, R. Ballesteros-Cillero, L. E. Ochando, K. Chulvi, R. Gotor, S. Gil, *Dyes Pigm.* **2019**, *160*, 198–207.

[26] E. Caruso, M. Gariboldi, A. Sangion, P. Gramatica, S. Banfi, *J. Photochem. Photobiol. B* **2017**, *167*, 269–281.

[27] T. Ozdemir, S. Atilgan, I. Kutuk, L. T. Yildirim, A. Tulek, M. Bayindir, E. U. Akkaya, *Org. Lett.* **2009**, *11*, 2105–2107.

[28] S. Choi, J. Bouffard, Y. Kim, *Chem. Sci.* **2014**, *5*, 751–755.

[29] R. P. Sabatini, B. Lindley, T. M. McCormick, T. Lazarides, W. W. Brennessel, D. W. McCamant, R. Eisenberg, *J. Phys. Chem. B* **2016**, *120*, 527–534.